Mem. S.A.It. Vol. 78, 92

Memorie della

Magnetic flux tubes observed with THEMIS/MSDP

P. Mein[1], N. Mein[1], M. Faurobert[2], G Aulanier[1], and J.-M. Malherbe[1]

[1] Observatoire de Paris-Section de Meudon, LESIA, F-92195 Meudon Cedex
[2] Université de Nice, UMR 6525, Parc Valrose, F-06108 Nice Cedex

Abstract. We use 2D spectro-polarimetric data of the NaD1 line to investigate magnetic flux tubes at several levels of the solar photosphere:
- magnetic and non-magnetic bright features can be discriminated by simple criteria of intensities and dopplershifts.
- 2D magnetic models and NLTE line profiles are compared to observations : combination of seeing effects and departures between slopes of line profiles in flux tubes and neighbouring photosphere account for vertical gradients of line-of-sight (LOS) magnetic field measurements.
- Best qualitative agreements are obtained with clusters of magnetic flux tubes.

Key words. Sun: atmosphere - Sun: magnetic fields

1. Observations

2D imaging spectro-polarimetry with THEMIS/MSDP (Mein, 2002) provided profiles of the NaD1 line across the active region NOAA 8989 on May 9, 2002. Line profile analysis was performed by the bisector method. Intensities, dopplershifts and line-of-sight (LOS) magnetic fields were determined in 4 locations defined by the distances from the bisector +/-0.008, +/-0.016, +/-0.024 and +/-0.032 nm. Subsequently, the measurements at +/-0.008 and +/-0.032 nm are called "core" and "wings" measurements respectively.

Figure 1 shows cuts (1) and (2) used in this analysis. Figures 2 and 3 show the LOS magnetic field deduced from the bisector method along both cuts (Berlicki at al., 2006).

Send offprint requests to: P.Mein, e-mail: Pierre.Mein@obspm.fr

Magnetic features A,B,C,D,E,F can be identified. In Figs. 4 and 5 showing brightness fluctuations, additional bright but non-magnetic featuress a,b,c,d,e,f are also present.

2. Discrimination by thermodynamical criteria

Magnetic and non-magnetic features can be discriminated by intensity and velocities measurements only. In Fig. 6, both kinds of features are displayed. Velocities measured in line wings at centres of features (peak values) are plotted versus differences between wing- and core-intensity fluctuations. We can see that magnetic features are displayed in the upper left part of the plot, and non-magnetic ones in the lower right part. Such discrimination might be used to analyse temperatures and velocities of magnetic structures by means of high reso-

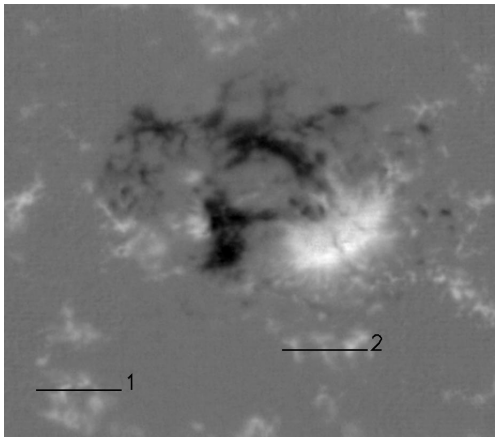

Fig. 1. LOS magnetic field at $\Delta\lambda$ = 0.024 nm and cuts (1) and (2) used in this paper. The field of view is 138"×121". North magnetic fields are white.

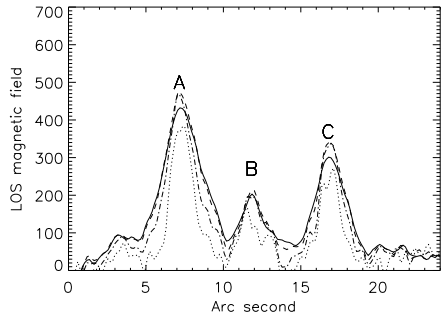

Fig. 2. Magnetic features along cut (1). Full lines refer to line-core measurements and dotted lines to line-wings .

lution data obtained without polarization analysis.

3. Mean spatial structure of magnetic features

By averaging LOS magnetic fields (Figs. 2 and 3) around symmetry axis of the six magnetic features A,B,C,D,E,F, we can derive a mean spatial structure. Figure 7 presents the LOS magnetic field versus the distance x to the axis.

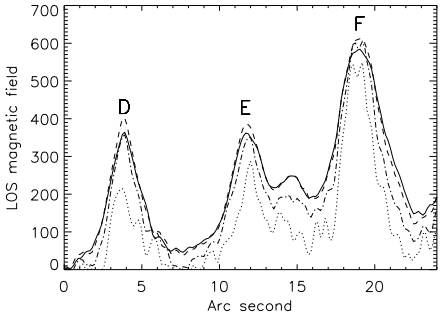

Fig. 3. Magnetic structures along cut (2) .

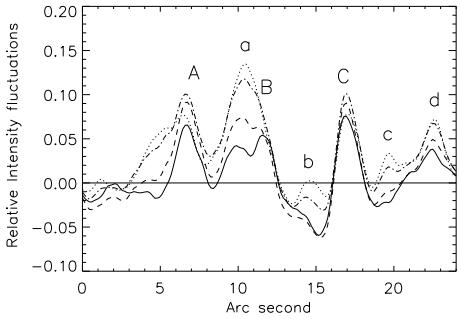

Fig. 4. Bright structures along cut (1) .

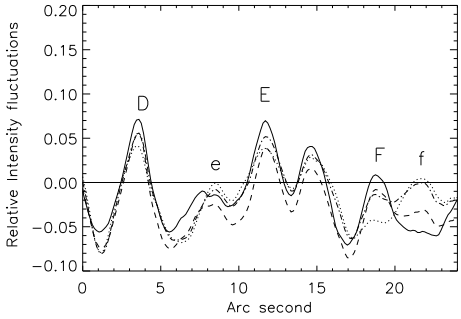

Fig. 5. Bright structures along cut (2) .

Crosses specify the half widths at half maximum (noted W).

We can notice that $W(wings) < W(core)$. This is expected because of the expansion of

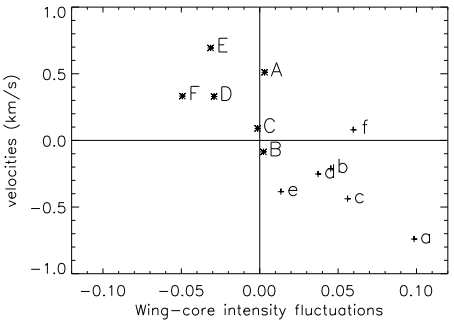

Fig. 6. Magnetic features A,B,C,D,E,F and non-magnetic features a,b,c,d,e,f in the diagram of wing-velocities versus differences between wing- and core-intensity .

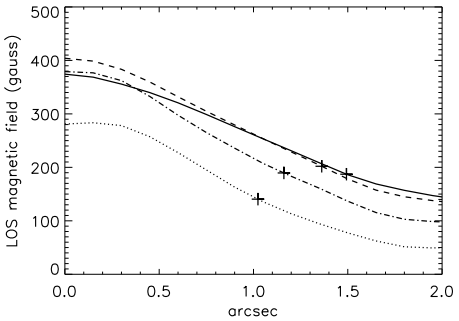

Fig. 7. Average observed magnetic features. Full line = line core; dotted line = line wing. .

magnetic lines from the lower levels to the upper levels of the photosphere.

But we must note also that the magnetic fields at $x = 0$ satisfy $B_0(wings) < B_0(core)$. That is not expected because the magnetic flux must be constant throughout the atmosphere. More detailed comparisons with flux-tube models and line transfer calculations will account for this point.

4. 2D model flux tube (I)

In the plane x, z we define the vertical component of the magnetic field along the symmetry axis by

$$B_z(0,z) = B_z(0,0) \cdot \exp(-z/h) \tag{1}$$

The horizontal variation of B_z inside the tube is defined by

$$B_z(x,z) = B_z(0,z) \cdot \cos^2(\pi x/(4d(z)) \tag{2}$$

$$-1 < x/2d(z) < 1 \tag{3}$$

To keep a constant flux versus z, we assume

$$d(z) = d(0) \cdot B_z(0,0)/B_z(0,z) \tag{4}$$

where $d(0)$ is the half width at half maximum of the tube, at the level $\tau_{5000} = 1$.

The horizontal magnetic field component is defined by the zero-divergence

$$\frac{\partial B_x(x,z)}{\partial x} = -\frac{\partial B_z(x,z)}{\partial z} \tag{5}$$

with

$$B_x(-\infty, z) = 0 \tag{6}$$

Figure 8 shows the model magnetic field (I) with

$$B_z(0,0) = 1100 \text{ G}$$
$$h = 240 \text{ km}$$
$$d(0) = 40 \text{ km}$$

We use the quiet solar VAL3C model (Vernazza et al., 1981) outside the flux tube. Inside the tube, we keep the same temperature at the same altitude, and modify all densities so that the total plasma pressure $P(x,z)$ (including the turbulent pressure) compensates the horizontal component of the Lorentz force. This ensures low departures from hydrostatic equilibrium.

5. Synthetic NaD_1 spectra of model (I)

The NaD_1 profiles are deduced from the 2.2 version of the NLTE radiative transfer code MULTI (Carlsson 1986). We use the assumption of weak magnetic field. At each altitude,

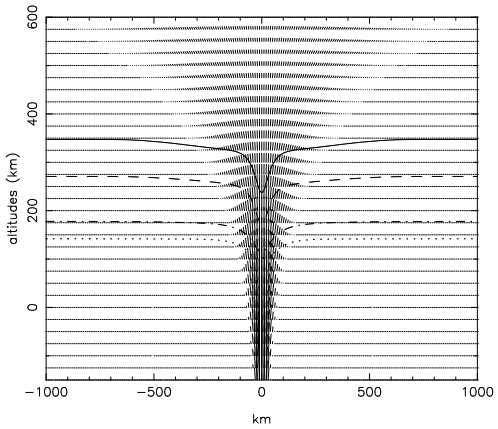

Fig. 8. 2D model magnetic field (I). Solid and dotted lines show formation altitudes of line core and line wings of the NaD_1 line .

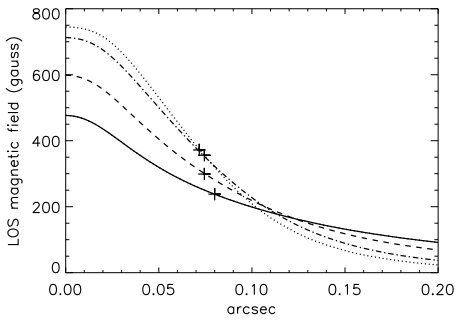

Fig. 9. Synthetic magnetic fields of model (I) .

the absorption coefficient in the line is translated by the corresponding Zeeman shift, for both Stokes profiles (I+V) and (I-V).

Synthetic LOS magnetic fields deduced from model (I) are plotted in Fig. 9. As in the case of observations, we see that $W(wings) < W(core)$, as expected from the expansion of flux tubes with height. But the magnetic field values at $x = 0$ satisfy the reverse inequality $B_0(wings) > B_0(core)$.

6. Model (I) with seeing effects

Seeing effects must be taken into account to mimic realistic observations. Along the x-axis,

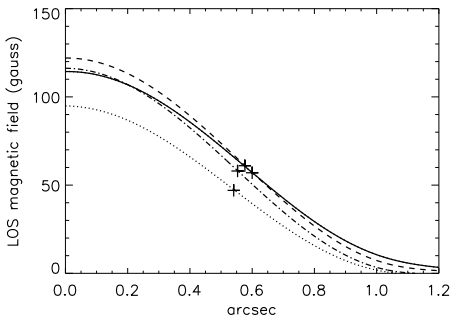

Fig. 10. Synthetic magnetic fields of model (I) with seeing effects .

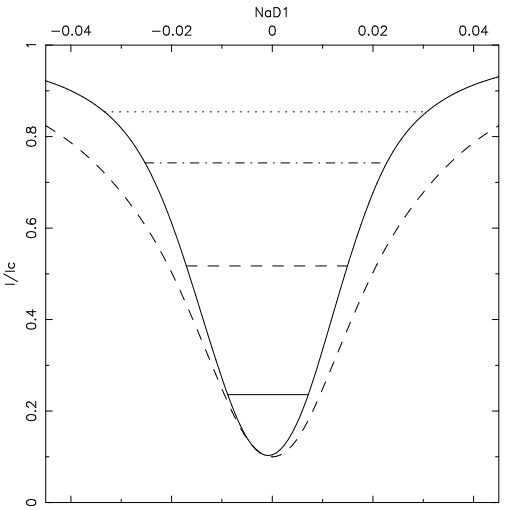

Fig. 11. *Full line*: NaD_1 profile on the axis of flux tube model (I); *dashed line*: quiet profile outside the tube .

we convolve the synthetic Stokes (I-V) intensities with the kernel

$$S(x) = \cos^2(\pi x/4s) \qquad -1 < x/2s < 1 \qquad (7)$$

for all wavelengths.

The synthetic magnetic fields corresponding to $s = 400$ km are plotted in Fig. 10. Both observational relationships $W(wings) < W(core)$ and $B_0(wings) < B_0(core)$ are now satisfied.

We can explain this behaviour in a simple way. Let us consider the line profile observed

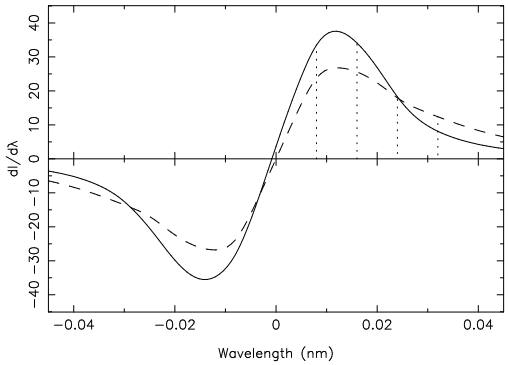

Fig. 12. slopes $dI/d\lambda$ of the line profile; *full line*: axis of flux tube; *dashed line*: quiet profile .

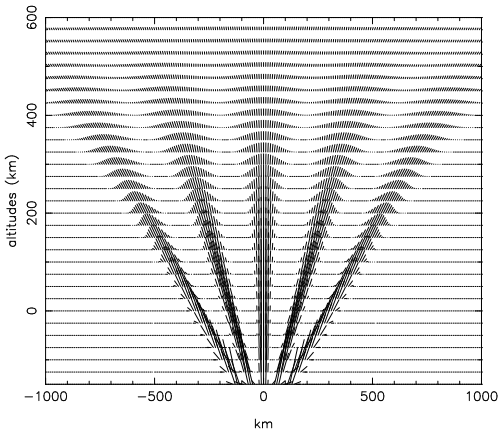

Fig. 13. Magnetic field of model (II) .

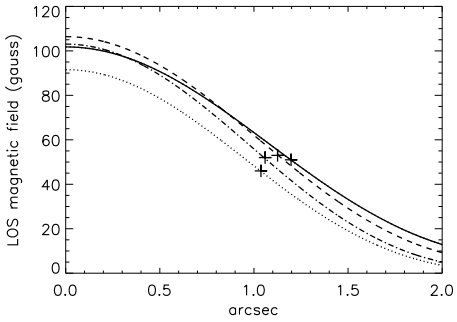

Fig. 14. Synthetic magnetic fields of model (II) with seeing effects .

at tube axis $I_{obs}(\lambda)$. If the width of the tube is small compared to the width of the seeing function $S(x)$, it can be roughly derived from the profile of the flux tube without seeing effects $I_{ft}(\lambda)$ (full line of Fig. 11) and from the quiet-sun profile $I_{qs}(\lambda)$ (dashed line of Fig. 11) by the equation

$$I_{obs}(\lambda) = f * I_{ft}(\lambda) + (1 - f) * I_{qs}(\lambda) \qquad (8)$$

where f is similar to a filling factor. Since intensity fluctuations equal the Zeeman shift times the slope of the line profile $dI/d\lambda$, we can write the following relationship between the observed magnetic fields $B_{obs}(\lambda)$ and the magnetic fields which should be observed without seeing effects $B_{ft}(\lambda)$

$$B_{obs}(\lambda) = B_{ft}(\lambda)/[1 + (1/f - 1)R] \qquad (9)$$

with

$$R = (dI/d\lambda)_{qs}/(dI/d\lambda)_{ft}. \qquad (10)$$

where $(dI/d\lambda)_{qs}$ and $(dI/d\lambda)_{ft}$ are the slopes of quiet-sun and flux-tube profiles respectively. Figure 12 shows $(dI/d\lambda)_{ft}$ (full line) and $(dI/d\lambda)_{qs}$ (dashed line). We can see that R decreases from the wings to the core of the line, which accounts for $B_{obs}(wings) < B_{obs}(core)$.

7. Cluster of inclined flux tubes (II)

The model (I) satisfies both observed qualitative relationships $W(wings) < W(core)$ and $B_0(wings) < B_0(core)$ (Figs. 7 and 10). But quantitative agreements should imply larger synthetic values of W_0 and B_0. Model (I) is not able to accept any increase of magnetic field, because the pressure reduction at high levels cannot exceed the pressure itself. A simple way to increase the amplitude of observed fields is to use clusters of flux tubes instead of single flux tubes. But a new difficulty arises. At high levels, where tubes are merging, the total field intensity exceeds the limit implied from gas pressure. It is possible to get round this difficulty by inclining flux tubes.

Figure 13 shows the magnetic model (II). Tube axes are straight lines.The central tube is vertical. At altitude zero, the widths of flux tubes are defined by $d(0)$, and the horizon-

tal distance between successive axes is 150 km. From one tube to the next, the inclination $\gamma = \partial x/\partial z$ increases by 0.6, so that the angles with the vertical direction are roughly 31 and 50 degrees. For each tube, we again keep Eqs. (2),(3),(4),(5), and (6), but we replace Eq. (1) by

$$B_z(x_0, z)^2 \cdot (1 + \gamma^2)/2\mu_0 = R \cdot P(-\infty, z) \quad (11)$$

where x_0 is the abscissa of tube axis at altitude z, R a ratio that does not depend on z, and $P(-\infty, z)$ the pressure of the quiet sun model. After adding the magnetic fields of all tubes, we define the total pressure by

$$\begin{aligned} P(x, z) &= P(-\infty, z) \\ &\quad -(B_x^t(x, z)^2 + B_z^t(x, z)^2)/2\mu_0 \end{aligned} \quad (12)$$

where B_x^t and B_z^t are the components of the total field. This condition, somewhat different from the condition used in model (I), also ensures low departures from hydrostatic equilibrium.

We choose the following parameters including seeing effects (Eq. 7):

$$R = 0.5$$
$$d(0) = 20 \text{ km}$$
$$s = 700 \text{ km}.$$

The synthetic magnetic fields are plotted in Fig. 14. Both relationships $W(wings) < W(core)$ and $B_0(wings) < B_0(core)$ are still satisfied. In addition, the order of magnitude of widths w is close to the observed values. The only condition that is not satisfied concerns the magnitude of observed fields. A ratio around 4 still remains between B_0 values of figures 7 and 14.

8. Conclusion

We analysed observations of facular features obtained with THEMIS/MSDP along the profile of NaD_1. We can deduce three main conclusions:

1) The detection of magnetic features can be performed by simple thermo-dynamical criteria using intensities and dopplershifts across the NaD_1 line.
2) The comparison with static magnetic flux tube models and NLTE synthetic profiles show that slopes of line profiles combined with seeing effects account for the apparent increase of LOS magnetic field between line wings and line core.
3) Clusters of flux tubes provide better agreement with observations than single flux tubes.

More details will be given in a forthcoming paper (Mein et al., 2007).

Further investigations should take into account more sophisticated models including velocities and temperature fluctuations, that could be deduced from observations taking into account point (1). 3D magnetic models of flux-tube clusters (point 3) should be also investigated for a better agreement with observations.

Acknowledgements. THEMIS is a French-Italian telescope operated on the island of Tenerife by CNRS-CNR in the Spanish Observatorio del Teide of the Instituto de Astrofisica de Canarias. We thank the THEMIS team who operates the telescope at Tenerife, and also C. Coutard and R. Hellier who performed many adjustments of the MSDP.

References

Berlicki, A., Mein, P. & Schmieder B., 2006, A&A 445, 1127.
Carlsson, M., 1986, Uppsala Astron. Obs. Report 33.
Mein, P., 2002, A&A, 381,271.
Mein, P., Mein, N., Faurobert, M., Aulanier, G. & Malherbe, J-M., 2007, A&A, in press.
Vernazza, J.E., Avrett, E.H., and Loeser, R., 1981, ApJ Suppl., 45,635.